



Wettability, microstructure and properties of 6061 aluminum alloy/304 stainless steel butt joint achieved by laser–metal inert-gas hybrid welding–brazing

Jun-yu XUE, Yuan-xing LI, Hui CHEN, Zong-tao ZHU

Key Laboratory of Advanced Technologies of Materials, Ministry of Education,
Southwest Jiaotong University, Chengdu 610031, China

Received 13 July 2017; accepted 26 February 2018

Abstract: Laser–metal inert-gas (MIG) hybrid welding–brazing was applied to the butt joint of 6061-T6 aluminum alloy and 304 stainless steel. The microstructure and mechanical properties of the joint were studied. An excellent joint-section shape was achieved from good wettability on both sides of the stainless steel. Scanning electron microscopy, energy-dispersive spectroscopy and X-ray diffractometry indicated an intermetallic compound (IMC) layer at the 6061-T6/304 interface. The IMC thickness was controlled to be $\sim 2 \mu\text{m}$, which was attributed to the advantage of the laser–MIG hybrid method. Fe_3Al dominated in the IMC layer at the interface between the stainless steel and the back reinforcement. The IMC layer in the remaining regions consisted mainly of $\text{Fe}_4\text{Al}_{13}$. A thinner IMC layer and better wettability on both sides of the stainless steel were obtained, because of the optimized energy distribution from a combination of a laser beam with a MIG arc. The average tensile strength of the joint with reinforcement using laser–MIG hybrid process was improved to be 174 MPa (60% of the 6061-T6 tensile strength), which was significantly higher than that of the joint by traditional MIG process.

Key words: welding–brazing; laser–metal inert-gas hybrid welding; butt joint; microstructure

1 Introduction

In recent years, lightweight composite structures have attracted attention because they can reduce environmental pollution and unnecessary energy waste [1–3]. In composite structure design, the aluminum–steel composite structure has exhibited excellent advantages and performance, and technology and a reliable quality of dissimilar aluminum–steel joints has been obtained [4,5]. However, the physical and the chemical properties of aluminum and steel, such as their melting point, thermal conductivity and expansion coefficient differ from each other. These differences could lead to a strong residual stress after welding. Excessive and complex Fe–Al intermetallic compounds (IMCs) such as FeAl , FeAl_3 , Fe_2Al and Fe_2Al_5 form [6]. These IMCs reduce joint quality because of their low toughness and high brittleness.

To avoid or reduce IMC formation, some researchers have concentrated on achieving dissimilar aluminum–steel joints by using solid-state welding

methods, such as friction stir welding [7], diffusion welding [8] and resistance spot welding [9]. However, the shape and size of such solid-state joints are restricted [10,11]. Welding–brazing has been studied as one of the main research directions to obtain dissimilar aluminum–steel joints. With welding–brazing process, the steel side with a high melting point is not melted, the liquid reaction between aluminum and steel can be inhibited, and thus the IMC layer thickness can be controlled efficiently.

In general, lap joints have been used to connect aluminum alloy and steel using welding–brazing. DONG et al [12] conducted welding experiments on lap joints of Al/steel by tungsten inert-gas (TIG) arc-welding–brazing with different-component filler wires, and investigated the effects of alloying elements on the microstructure of the weld, and tensile strength of the resultant joint. LI et al [13] studied the effect of pulse-on-pulse frequency on the welding process and quality by pulse-on-pulse metal inert-gas (MIG) welding–brazing. However, joint overlap increases the mass of the dissimilar structure. Therefore, ZHANG et al [5] conducted an aluminum and

steel butt-joint experiment by micro-gap laser-welding–brazing with a coaxial powder-feeding method. Usually, the poor rear heated of Al/steel butt joint was one of the most serious problems, and it is difficult to obtain Al/steel butt joints of good quality. Therefore, YE et al [14] conducted MIG–TIG double-sided arc welding–brazing to join aluminum and stainless steel, and a sound welding–brazing joint with excellent front and back formation was achieved. However, MIG–TIG double-sided arc-welding–brazing was restricted from welded structures without a rear space.

Laser–MIG hybrid welding is reliable and efficient, can improve the efficiency of the arc heat source and can increase welding penetration without excessive heat input. For the laser–MIG hybrid welding–brazing of an aluminum–steel butt joint, rear heating can be improved by a high-energy laser, and an excellent front formation can be achieved from the advantages of MIG. However, Al/steel butt joints have rarely been reported when using laser–MIG hybrid welding–brazing.

A laser–MIG hybrid welding–brazing process was developed for a 6061-T6/304 butt joint without a groove and gap. The wettability of melted aluminum alloy on the surface of stainless steel by laser–MIG hybrid process was investigated by measuring the wetting angles from an optical microscope photo of the joint. The microstructure, especially the IMC structure at the interface, was characterized by analyzing components from scanning electron microscope (SEM) images and the X-ray diffractometry (XRD) pattern of the fracture surface. The tensile strength and joint microhardness were evaluated and the joint-fracture mechanism was analyzed.

2 Experimental

Plates of 6061-T6 aluminum alloy and 304 stainless steel (both 2 mm-thick) were cut to 100 mm × 50 mm. The filler metal was 1.2 mm-in-diameter ER4043 aluminum alloy wire (Al–5Si). Because the gap and groove were not set up for this experiment, and the flow of the filler metal toward the bottom of joint may be difficult, an Al–Si–Mg foil interlayer (110 mm × 2 mm × 0.1 mm) was placed between the butt planes of two base metals to avoid a shortage of molten metal at the bottom of the weld, which also contributed to restrain the growth

of the IMC layer at the interface between the stainless steel and the weld seam by the addition of Si element [10,12]. The nominal chemical compositions of aluminum alloy, stainless steel, filler wire and interlayer are listed in Table 1. Before welding, the test-piece surfaces were polished by abrasive paper to remove the oxide film, and they were cleaned using acetone and dried. Non-corrosive (Nocolok) flux, which is composed of $KAlF_4$, was used to improve the molten metal wettability on the steel surface. The flux was dissolved in acetone and spread homogeneously on the steel surface to be ~0.3 mm in thickness.

An IPG YSL–4000 fiber laser with a maximum power output of 4 kW and a KEMPPI kempArc–405 digital welding machine were used. A paraxial laser–MIG hybrid mode in which a laser guiding arc was applied and a paraxial welding torch was assembled by an IRB2600 robot, was used. A schematic of the welding process is shown in Fig. 1. A laser beam of 1070 nm in wavelength was focused on the workpiece surface of 310 mm in focal length and its focal spot diameter was ~0.2 mm. To reduce the laser reflection on the aluminum alloy plate, the laser beam was irradiated on the aluminum alloy plate surface at 80°, and the angle between the laser beam and the MIG torch was 15°. The laser focal point and MIG torch offset were used to avoid melting the steel, and the offset distance from the joint center line toward the side of the aluminum was ~0.5 mm. The distance between the laser focal point and the filler wire was 2–3 mm. Argon gas (99.999%) was used as a shielding gas to avoid melt-pool oxidation. The optimal laser–MIG hybrid and MIG welding–brazing parameters are listed in Table 2.

Standard samples (12 mm × 12 mm) were cut from a test piece along the weld cross section, polished, and etched using Keller reagent. The macro-appearance and weld microstructure were studied by using a JENOPTIK stereomicroscope and a SU8010 SEM, respectively, and the elemental contents of the weld were analyzed by energy-dispersive spectroscopy (EDS).

Three tensile samples of the same weld were tested with dimensions as shown in Fig. 2. The tensile test was measured with a loading speed of 1 mm/min by a CMT4304 mechanical machine, and the fractured surfaces of the tensile samples were observed and analyzed by SEM, EDS and Pro-MPD XRD. A Vickers

Table 1 Chemical compositions of experimental materials (mass fraction, %)

Material	Si	Cr	Ni	Mg	Mn	C	Zn	Ti	Al	Fe
304	≤0.1	17.0–20.0	8.0–10.5	–	≤0.2	≤0.08	–	–	–	Bal.
6061-T6	0.4–0.8	0.10–0.35	–	1.0	0.15	–	0.25	0.1	Bal.	0.7
ER4043	4.5–6.0	–	–	≤0.05	≤0.05	–	≤0.1	0.1	Bal.	≤0.6
Al–Si–Mg	16.96	–	–	1.31	–	–	–	–	81.83	–

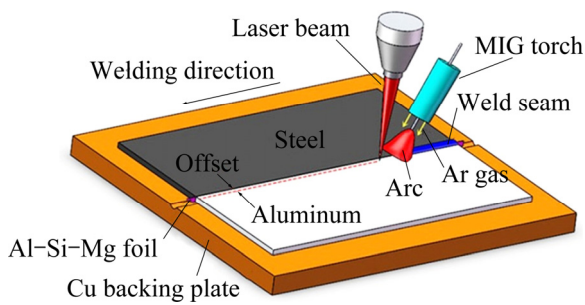


Fig. 1 Schematic diagram of laser-MIG hybrid welding-brazing

Table 2 Welding parameters

Process	Laser power/ W	Welding speed/ (mm·s ⁻¹)	Feeding speed/ (m·min ⁻¹)	Defocusing value/ mm	Ar gas flow rate/ (L·min ⁻¹)
Laser-MIG	1000	17	4.5	+4.5	25
MIG	–	17	4.5	–	25

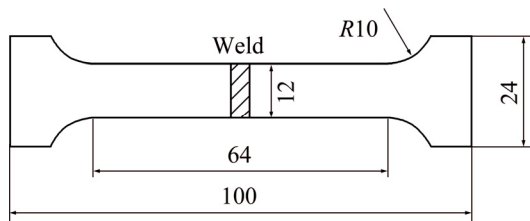


Fig. 2 Schematic diagram of tensile test sample (unit: mm)

microhardness test was used to measure the microhardness at different regions of the joint by using the HXD-1000TM digital microhardness tester with a 300 g load for 15 s. The distance between the two test points was 250 μm.

3 Results and discussion

3.1 Wettability and weld forming

A sound weld appearance with good front and back formation could avoid stress concentration, and enhance the joint mechanical properties. Figures 3(a) and (b) show the surface appearance of the aluminum/steel dissimilar butt joints using laser-MIG hybrid welding-brazing. A continuous and smooth front and back formation without cracks and excessive spatters was obtained, which implies that the welding process is stable and reliable. However, massive spatters and unstable rear forming were found in the joint obtained by the traditional MIG process, as shown in Figs. 3(d) and 3(e). Some research has shown that it is difficult for aluminum droplets to spread and develop metallic bonding for uncoated steel [15,16], and especially aluminum droplets are hard to wet and spread on the rear of the steel because of insufficient heating using a conventional arc process. In the traditional MIG process, an invalid rear spreading was found, as shown in Fig. 3(f). The typical cross-section of the aluminum-steel dissimilar butt joint by laser-MIG hybrid process is shown in Fig. 3(c). This indicates that better wetting and spreading on the upper and rear side of the stainless steel was achieved, and that the wetting angles of the upper and the rear side of

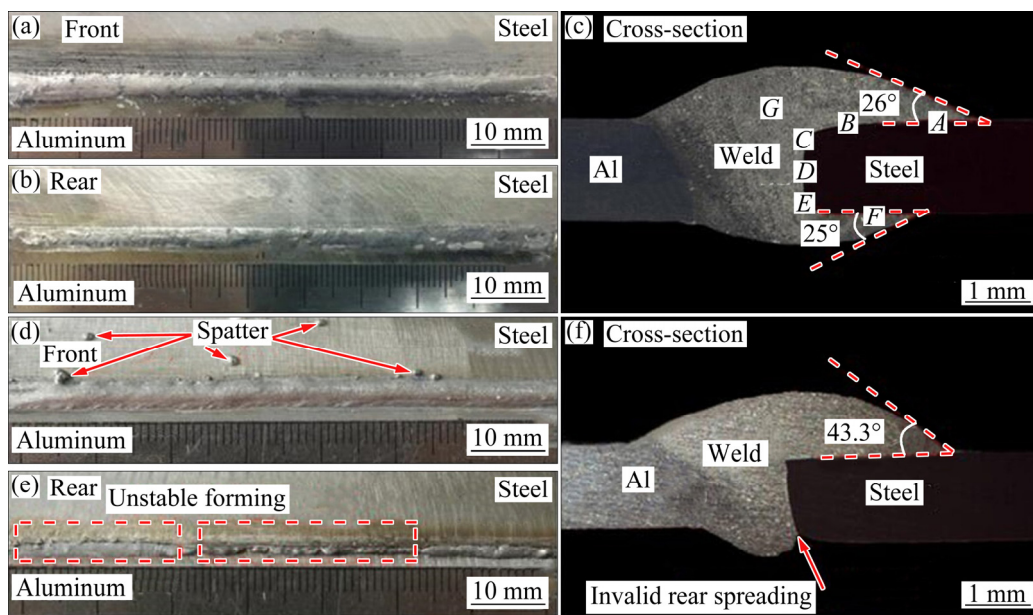


Fig. 3 Appearances and typical cross-section morphologies of aluminum-steel dissimilar butt joint: (a–c) Front appearance, rear appearance and cross-section of joint by laser-MIG hybrid process; (d–f) Front appearance, rear appearance and cross-section of joint by MIG process

the stainless steel were 26° and 25°, respectively. In laser–MIG hybrid process, although uncoated stainless steel was chosen as base metal, the molten metal spread well on the front and rear of the stainless steel, and the wetting and spreading of the joint back was improved considerably, which is attributed to a reasonable energy distribution of the laser–MIG hybrid heat source.

3.2 Interface microstructure

The mechanical properties of the joint depend on the type, morphology and thickness of the IMCs [17,18]. It is necessary to analyze the IMC-layer microstructure in detail. Figure 4 shows the interface microstructure of joint by laser–MIG hybrid process in different regions with A–F marked in Fig. 3(c).

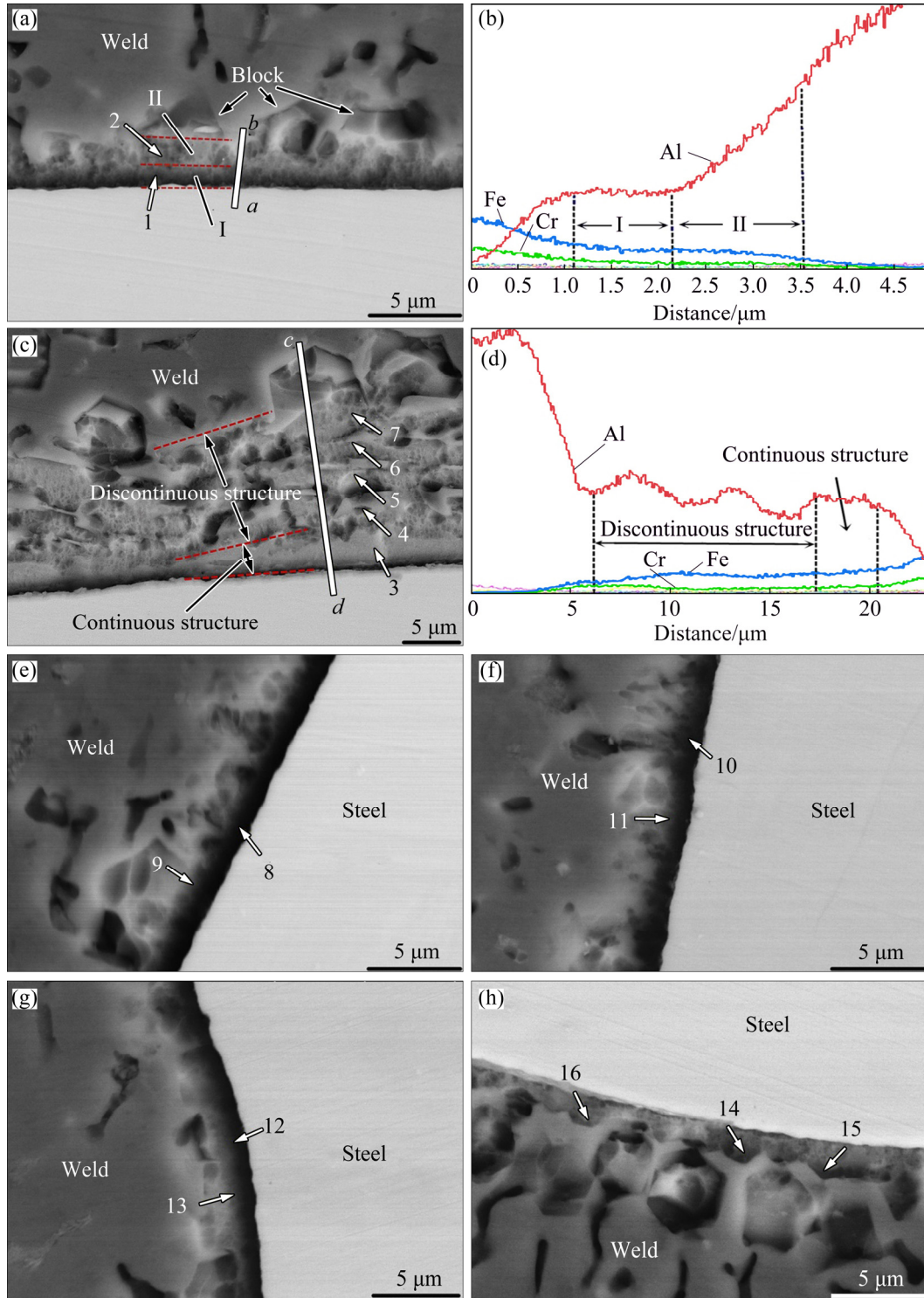


Fig. 4 Microstructures of interface in different regions in Fig. 3(c): (a) Region A; (b) Line scanning from a to b; (c) Region B; (d) Line scanning from c to d; (e) Region C; (f) Region D; (g) Region E; (h) Region F

Figures 4(a) and 4(c) show the interface microstructure at the upper region of the joint. In region *A*, the thickness of interface layer was $\sim 2.5 \mu\text{m}$. The interface layer can be divided into two layers (layers I and II), as shown in Fig. 4(a). EDS linear scanning along the line (from *a* to *b*) was used to analyze the compositions of layers I and II. The results show that the main elements of the interface layers were Al, Fe and Cr. In layer I, the compositions of Al, Fe and Cr were stable, but the Al content increased gradually, whereas the Fe and Cr contents decreased in layer II, as shown in Fig. 4(b). The content variety of Al, Fe and Cr in layers I and II indicates that the metallurgical bonding occurred at the interface between the weld seam and the steel surface, and the Fe–Al IMCs may exist in the interface layer. EDS region analysis was performed at locations 1 and 2, with the results listed in Table 3. Fe atoms can be replaced by Cr and Ni [19] to form $\text{Fe}(\text{Cr},\text{Ni})_x\text{Al}_y$, and thus IMC in layers I and II may both consist of $\text{Fe}_4\text{Al}_{13}$. Compared with layer II, the structure of $\text{Fe}_4\text{Al}_{13}$ in layer I was more uniform and compact, and the $\text{Fe}_4\text{Al}_{13}$ in layer II nucleated on layer I and grew toward the weld as a flocculent structure. Some block structures were found near layer II, which may be $\alpha_c\text{-AlFeSi}$. A similar phenomenon had been reported by LEONARDO et al [20]. The microstructure of region *B* is shown in Fig. 4(c). A thicker ($\sim 15 \mu\text{m}$ -thick) interface layer was caused by excessive heat input. A compact and continuous structure formed near the steel side, and a complex and discontinuous structure was piled on the

continuous structure. EDS linear scanning along the line (from *c* to *d*) indicated that the Fe and Cr contents were stable, and that fluctuation in Al content was caused by the $\alpha(\text{Al})$ in the discontinuous structure, as shown in Fig. 4(d). Massive IMCs existed in this interface layer. Components at locations 3–7 were analyzed by EDS region analysis, with the results listed in Table 3, and the continuous and discontinuous structure may be $\text{Fe}_4\text{Al}_{13}$.

Similarly, the interface of the butt plane between the weld seam and the steel surface consists of Fe–Al IMCs, which indicates that the metallurgical bonding occurred at the interface. Figures 4(e–g) show the IMC microstructures at the butt plane of the joint, which correspond to regions *C–E*, respectively. The IMC layer in regions *C–E* was $\sim 2 \mu\text{m}$ -thick, and presented similar microstructure characteristics to region *A*. In contrast with the IMC layer that is located in region *A*, the IMC-layer thickness in regions *C–E* was thinner. Layer I dominated the entire IMC layer whereas growth of layer II was constrained. This behavior is attributed to the lower heating and faster cooling at the butt plane. EDS analysis in Table 3 shows that the IMC layer in regions *C–E* may consist of $\text{Fe}_4\text{Al}_{13}$, which is the same as that in region *A*.

Figure 4(h) presents the IMC microstructures at the bottom of the joint, corresponding to region *F* in Fig. 3(c). The morphology and structure of the IMCs in region *F* differed from the other regions. The IMC layer thickness was $\sim 1.5 \mu\text{m}$. The EDS analysis results are listed in Table 3, and indicate that the IMC layer may consist of Fe_3Al , which differed from other reports [14,17,21]. The formation of Fe_3Al improves the joint quality because of its reduced brittleness.

In summary, the IMC layer thickness was controlled to be $\sim 2 \mu\text{m}$, except for region *B*, which was much thinner than the critical value in Ref. [22]. The IMC layer at the bottom of the joint consists of Fe_3Al . The remaining regions consist mainly of $\text{Fe}_4\text{Al}_{13}$.

3.3 Microstructure of weld seam

Figure 5 shows the microstructure of the weld seam of region *G* in Fig. 3(c) and the EDS analysis results are given in Table 4. $\alpha(\text{Al})$ dominated in the weld seam. The Al–Si eutectic phase appeared in the weld seam as labeled at locations 18 and 19. Fe atoms were mixed partially into the Al–Si eutectic to form a Fe–Al–Si ternary compound, which appeared as dendrite-like or net-like dark structures in Fig. 5 and is labeled as locations 20–22.

3.4 Mechanical properties

A tensile test was carried out to evaluate the tensile strength of the 6061-T6/304 butt joint using laser–MIG

Table 3 EDS analysis results of locations 1–16 in Fig. 4

Location	$x(\text{Al})/\%$	$x(\text{Fe}+\text{Cr}+\text{Ni})/\%$	$x(\text{Si})/\%$
1	74.10	23.62	1.79
2	81.71	16.97	0.71
3	75.18	22.29	2.16
4	80.22	17.29	1.95
5	75.48	19.54	4.78
6	77.52	16.85	5.46
7	80.31	15.68	3.42
8	72.36	23.17	4.03
9	80.04	17.66	1.95
10	75.17	23.25	1.59
11	80.11	15.16	2.98
12	71.65	23.24	4.95
13	78.75	16.00	5.15
14	28.15	69.55	0.33
15	37.45	60.56	0.14
16	27.89	70.15	0.20

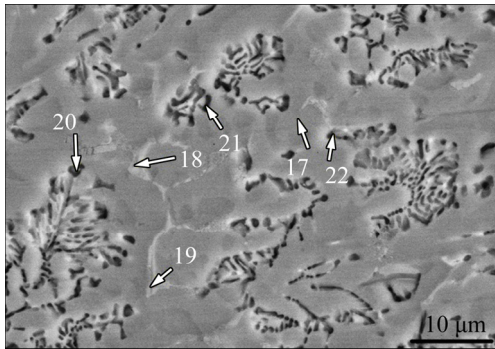


Fig. 5 Microstructure of weld seam by laser-MIG hybrid process

Table 4 EDS region analysis results of locations 17–22 in Fig. 5

Location	x(Al)/%	x(Fe)/%	x(Si)/%
17	96.41	0.15	1.68
18	83.90	1.78	12.27
19	85.4	2.28	10.60
20	78.57	7.59	11.02
21	79.58	7.37	12.47
22	88.71	4.50	6.51

hybrid welding-brazing. For the joint without reinforcement, the failure occurred at the IMC layer between stainless steel and the weld seam. As shown in Fig. 6, the average tensile strength of the joint without reinforcement by laser-MIG hybrid method was 154 MPa, which was significantly higher than that of the joint by traditional MIG process. The addition of the laser beam improves the energy distribution of joint, and makes sure that the rear of joint is heated efficiently. With a fast welding speed, a uniform and thin IMCs layer was obtained, and thus a better tensile strength of joint was achieved using laser-MIG hybrid process than that of the joint by MIG process.

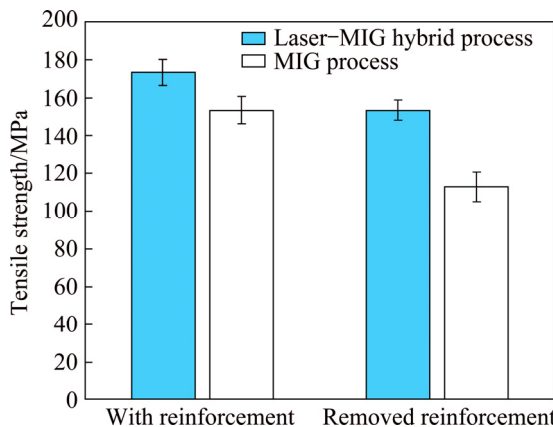


Fig. 6 Tensile strength of butt joint by two different processes

For the joint with reinforcement, benefited from the better mechanical strength of IMC layer in laser-MIG hybrid method, the average tensile strength of the joint with reinforcement by laser-MIG hybrid method was improved to be 174 MPa, which was also obviously superior to that by traditional MIG method. The fracture location of the joint with reinforcement by laser-MIG hybrid process is shown in Fig. 7. During the tensile test, a crack occurred firstly in the IMC layer of the butt plane, then propagated to the weld metal at the bottom and the upper of the joint, and finally, led to the fracture of the joint. SEM photographs of the fracture surface of the joint are shown in Fig. 8. The weld metal of the upper and lower region presents the ductile fracture mode, as shown in Figs. 8(c) and (d), but the IMC region presents a typical cleavage fracture mode with a river pattern, as shown in Fig. 8(b). To confirm the phase on the crack surface of the IMC region, XRD analysis was performed before the front and rear crack-surface reinforcements had been removed. The result is shown in Fig. 9. Fe₄Al₁₃ existed on the IMC region surface, and the result is consistent with the previous EDS analysis.

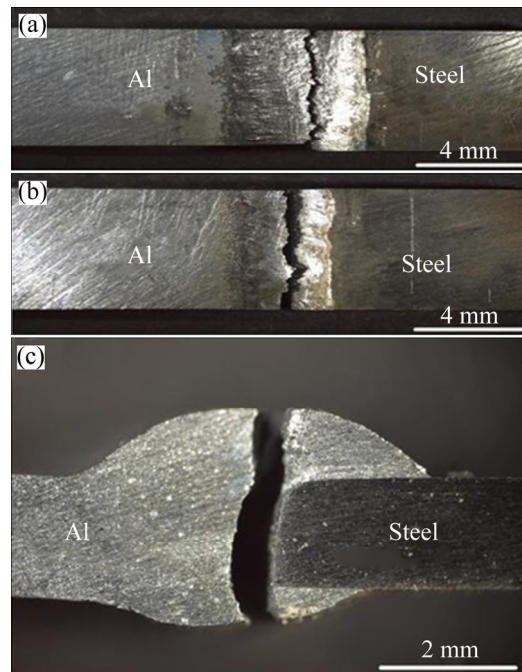


Fig. 7 Fracture location of joint by laser-MIG hybrid process: (a) Front appearance; (b) Rear appearance; (c) Cross-section

The Vickers microhardness test was carried out to measure the microhardness of the joint by laser-MIG hybrid process in different regions. As shown in Fig. 10, three microhardness curves exhibited the same change, and stabilized near HV 100 in the weld seam. This result indicates that the weld seam was homogeneous in composition and structure. The microhardness in the

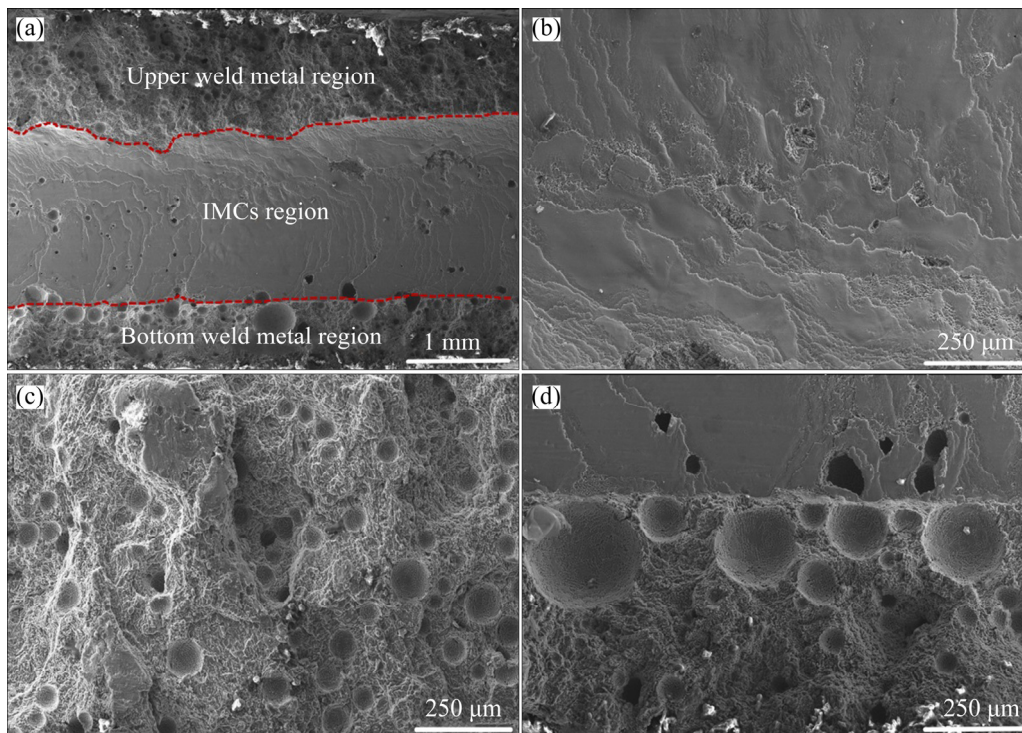


Fig. 8 SEM fractographies of joint: (a) Entire joint morphology; (b) Enlarged IMC region; (c) Enlarged upper weld metal region; (d) Enlarged bottom weld metal region

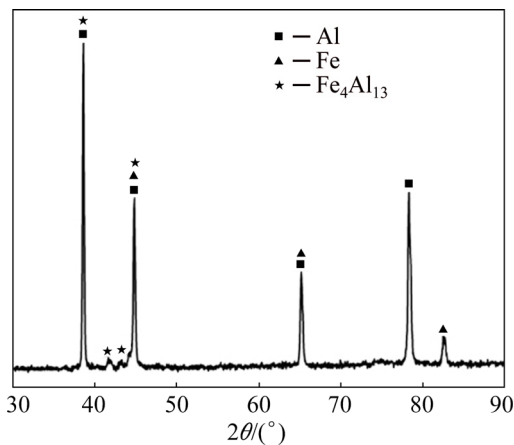


Fig. 9 XRD pattern of fracture surface

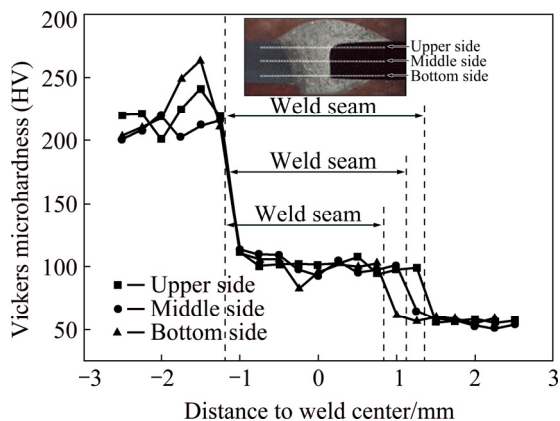


Fig. 10 Microhardness of joint by laser-MIG hybrid process in different regions

weld seam was lower than that of the steel side, and was significantly higher than that of the aluminum alloy side. Based on SEM and EDS analysis for the weld seam, Fe atoms were mixed into the weld seam and formed a Fe–Al–Si ternary structure, which was harder than the α (Al). The ternary structure was distributed uniformly in the weld seam, which enhanced the weld seam microhardness. Because the IMC layer between the steel side and the weld seam was too thin, the microhardness of the IMC layer was not obtained.

4 Conclusions

1) Compared with the traditional MIG process, the laser-MIG hybrid welding-brazing process could achieve a sound welding-brazing butt joint of 6061-T6/304 with excellent front and rear formation. The molten metal had a good wettability on the 304 stainless steel surface and could spread well on the rear of the joint using the laser-MIG hybrid welding-brazing method.

2) The thickness and microstructure of the IMC layer at different regions of the joint varied because of different heating and cooling conditions. For the IMC layer of 6061-T6/304 butt joint using laser-MIG hybrid welding-brazing process, in the upper region, the IMC layer consisted of compact layer I and flocculent layer II, which were both Fe_4Al_{13} . At the butt plane, the IMC

layer showed a similar microstructure to that in the upper region, but the growth of layer II was restrained and the IMC layer became thinner. Fe_3Al existed at the back of the joint, which resulted in a thin IMC layer at the back region. The average thickness of the IMC layer was controlled to be $\sim 2 \mu\text{m}$. The weld metal microstructure consisted of $\alpha(\text{Al})$, Al–Si eutectic structure and Fe–Al–Si ternary compound.

3) Because of the uniform and thin IMCs layer without any crack, an average tensile strength of the joint with reinforcement using laser–MIG hybrid process was improved to be 174 MPa (60% of the 6061-T6 tensile strength), which was obviously better than that by traditional MIG process. The fracture of joint with reinforcement using laser–MIG hybrid process was initiated in the $\text{Fe}_4\text{Al}_{13}$ layer of the butt plane in typical cleavage fracture mode, and propagated to the weld metal at the front and rear reinforcement of the joint.

4) Because of the formation of Fe–Al IMCs in the weld seam by laser–MIG hybrid process, the strength in this region was enhanced such that the microhardness was higher than that of the aluminum alloy.

References

- [1] SU Yong-chao, HUA Xue-ming, WU Yi-xiong. Effect of input current modes on intermetallic layer and mechanical property of aluminum–steel lap joint obtained by gas metal arc welding [J]. *Materials Science and Engineering A*, 2013, 578(31): 340–345.
- [2] KATAYAMA S. Laser welding of aluminum alloys and dissimilar metals [J]. *Welding International*, 2004, 18(8): 618–625.
- [3] TORKAMANY M J, TAHAMTAN S, SABBAGHZADEH J. Dissimilar welding of carbon steel to 5754 aluminum alloy by Nd:YAG pulsed laser [J]. *Materials and Design*, 2010, 31(1): 458–465.
- [4] STAUBACH M, JUTTNER S, FUSSEL U, DIETRICH M. Joint of steel–aluminum mixed joints with energy-reduced GMA processes and filler materials on an aluminum and zinc basis [J]. *Welding and Cutting*, 2008, 7(1): 30–38.
- [5] ZHANG Yi, LI Fu-nan, GUO Guo-liang, WANG Gang, WEI Hai-ying. Effects of different powders on the micro-gap welding-brazing of an aluminum–steel butt joint using a coaxial feeding method [J]. *Materials and Design*, 2016, 109(5): 10–18.
- [6] ASM International. Binary alloy phase diagrams [M]. Metals Park, ASM International, 1996.
- [7] LIU Xun, LAN Shu-huai, NI Jun. Analysis of process parameters effects on friction stir welding of dissimilar aluminum alloy to advanced high strength steel [J]. *Materials and Design*, 2014, 59(6): 50–62.
- [8] SHI H X, QIAO S, QIU R F. Effect of welding time on the joint phenomena of diffusion welded joint between aluminum alloy and stainless steel [J]. *Material Manufacturing Process*, 2012, 27(12): 1366–1369.
- [9] ZHANG W H, QIU X M, SUN D Q. Effects of resistance spot welding parameters on microstructures and mechanical properties of dissimilar material joints of galvanized high strength steel and aluminum alloy [J]. *Science and Technology of Welding and Joining*, 2010, 16(2): 153–161.
- [10] LIN S B, SONG J L, YANG C L, FAN C L, ZHANG D W. Brazability of dissimilar metals tungsten inert gas butt welding-brazing between aluminum alloy and stainless steel with Al–Cu filler metal [J]. *Materials and Design*, 2010, 31(5): 2637–2642.
- [11] ZHANG Yu-feng, HUANG Ji-huang, CHENG Zhi, YE Zheng, CHI Hai. Study on MIG-TIG double-sided arc welding-brazing of aluminum and stainless steel [J]. *Materials Letters*, 2016, 172(1): 146–148.
- [12] DONG Hong-gang, HU Wen-jin, DUAN Yu-ping, WANG Xu-dong, DONG Chuang. Dissimilar metal joining of aluminum alloy to galvanized steel with Al–Si, Al–Cu, Al–Si–Cu and Zn–Al filler wires [J]. *Journal of Materials Processing Technology*, 2012, 21(2): 458–464.
- [13] LI Jian-xiong, LI Huan, WEI Hui-liang, NI Yan-bing. Effect of pulse on pulse frequency on welding process and welding quality of pulse on pulse MIG welding-brazing of aluminum alloys to stainless steel [J]. *International Journal of Advanced Manufacturing Technology*, 2016, 87(1–4): 1–13.
- [14] YE Zheng, HUANG Ji-huang, GAO Wei, ZHANG Yu-feng, CHENG Zhi. Microstructure and mechanical properties of 5052 aluminum alloy/mild steel butt joint achieved by MIG-TIG double-sides arc welding-brazing [J]. *Materials and Design*, 2017, 123(5): 69–79.
- [15] CHEN Shu-hai, LI Li-qun, CHEN Yan-bing, HUANG Ji-hua. Joining mechanism of Ti/Al dissimilar alloys during laser welding-brazing process [J]. *Journal of Alloys and Compounds*, 2011, 509(3): 891–989.
- [16] SUN J H, HUANG J, YAN Q, LI Z. Fiber laser butt joining of aluminum to steel using welding-brazing method [J]. *International Journal of Advanced Manufacturing Technology*, 2016, 85(9–12): 2639–2650.
- [17] SUN Jun-hao, YAN Qi, LI Zhu-guo, HUANG Jian. Effect of bevel angle on microstructure and mechanical property of Al/steel butt joint using laser welding-brazing method [J]. *Materials and Design*, 2016, 90(15): 468–477.
- [18] BOUAYAD A, CEROMETTA C, BELKEBIR A, AMBARI A. Kinetic interactions between solid iron and molten aluminum [J]. *Materials Science and Engineering A*, 2003, 363(1–2): 53–61.
- [19] YANG Jin, LI Yu-long, ZHANG Hua. Microstructure and mechanical properties of pulsed laser welded Al/steel dissimilar joint [J]. *Transactions of Nonferrous Metals Society of China*, 2016, 26(4): 994–1002.
- [20] LEONARDO A, SEBASTIAN W, ALOIS L. Influence of filler composition on the microstructure and mechanical properties of steel-aluminum joints produced by metal arc joining [J]. *Advanced Engineering Materials*, 2009, 11(5): 350–358.
- [21] QIN Guo-liang, JI Yang, MA Hong, AO Zhi-yong. Effect modified flux on MIG arc brazing-fusion welding of aluminum alloy to steel butt joint [J]. *Journal of Materials Processing Technology*, 2017, 245: 115–121.
- [22] CAO R, HUANG Q, CHEN JH, WANG P C. Cold metal transfer spot plug welding of AA6061-T6-to-galvanized steel for automotive applications [J]. *Journal of Alloys and Compounds*, 2014, 585(3): 622–632.

6061 铝合金/304 不锈钢激光-金属惰性气体复合熔钎焊 对接接头润湿性、显微组织及性能

薛珺予, 李远星, 陈 辉, 朱宗涛

西南交通大学 材料先进技术教育部重点实验室, 成都 610031

摘 要: 采用激光-金属惰性气体(MIG)复合熔钎焊的方法实现 6061-T6 铝合金与 304 不锈钢异种金属对接接头的焊接, 并研究焊后接头的显微组织和力学性能。由于熔融金属在不锈钢两侧润湿铺展良好, 焊后接头具有良好的截面形貌。采用扫描电镜、能谱仪及 X 射线衍射仪表征 6061-T6/304 界面的金属间化合物(IMC)层。结果表明, 基于激光-MIG 复合焊的优势, IMC 层的整体厚度被控制在 2 μm 左右, 位于不锈钢和接头背部余高之间的 IMC 层的组织主要为 Fe_3Al , 位于其他位置的 IMC 层的组织主要为 $\text{Fe}_4\text{Al}_{13}$ 。由于激光束与 MIG 电弧热源的结合能够有效优化热源分布, 焊后接头的 IMC 层厚度较薄, 同时, 熔融金属在不锈钢两侧具有良好的润湿铺展。焊后带有余高的接头的抗拉强度可达 174 MPa, 约为 6061 母材强度的 60%, 明显高于传统单一 MIG 热源作用下的接头的抗拉强度。

关键词: 熔钎焊; 激光-MIG 复合焊; 对接接头; 显微组织

(Edited by Bing YANG)